Structure, Vol. 9, 215–220, March, 2001, ©2001 Elsevier Science Ltd. All rights reserved. PII S0969-2126(01)00578-0

Three-Dimensional Structure of a Voltage-Gated Potassium Channel at 2.5 nm Resolution

Olga Sokolova,* Ludmila Kolmakova-Partensky,† and Nikolaus Grigorieff†‡
*W. M. Keck Institute for Cellular Visualization
Rosenstiel Basic Medical Research Center
†Department of Biochemistry
Howard Hughes Medical Institute
Brandeis University
Waltham, Massachusetts 02454

Summary

Background: The voltage-gated potassium channel Shaker from *Drosophila* consists of a tetramer of identical subunits, each containing six transmembrane segments. The atomic structure of a bacterial homolog, the potassium channel KcsA, is much smaller than Shaker. It does not have a voltage sensor and other important domains like the N-terminal tetramerization (T1) domain. The structure of these additional elements has to be studied in the more complex voltage-gated channels.

Results: We determined the three-dimensional structure of the entire Shaker channel at 2.5 nm resolution using electron microscopy. The four-fold symmetric structure shows a large and a small domain linked by thin 2 nm long connectors. To interpret the structure, we used the crystal structures of the isolated T1 domain and the KcsA channel. A unique density assignment was made based on the symmetry and dimensions of the crystal structures and domains, identifying the smaller domain as the cytoplasmic mass of Shaker containing T1 and the larger domain as embedded in the membrane.

Conclusions: The two-domain architecture of the Shaker channel is consistent with the recently proposed "hanging gondola" model for the T1 domain, putting the T1 domain at a distance from the membrane domain but attached to it by thin connectors. The space between the two domains is sufficient to permit cytoplasmic access of ions and the N-terminal inactivation domain to the pore region. A hanging gondola architecture has also been observed in the nicotinic acetylcholine receptor and the KcsA structure, suggesting that it is a common element of ion channels.

Introduction

Until recently, most of our knowledge of how ion channels work was derived solely from electrophysiology and mutagenesis [1]. Recently, the atomic structures of the bacterial potassium channel KcsA [2] and the T1 domain [3] were determined. The structure of KcsA shows for the first time how ion selectivity can be realized by tetrameric coordination of ions in the channel pore. The structure of KcsA also offers answers to how a charged particle can be stabilized in the middle of the hydrophobic lipid bilayer [4]. However, other common elements of ion channels, such as voltage sensor and regulatory domains, are not present in KcsA and have to be studied in other channels such as Shaker.

The Shaker potassium channel is the most thoroughly studied voltage-gated ion channel, and extensive mutagenesis has been carried out to gain insight into its structure and function [1]. Sequence analysis of the Shaker gene predicts six hydrophobic and α-helical transmembrane segments termed S1–S6. The N-terminal domain includes a so-called tetramerization, or T1, domain. Shaker-type potassium channels remain functional when most of the N-terminal domain is removed [5]. The structure of the channel pore, formed by segments S5, S6, and P, is now known in atomic detail from the structure of the largely homologous bacterial KcsA channel. The cytoplasmic T1 domain forms a tetramer in isolation [3] and in the fully assembled channel [6]. Following activation, the inactivation peptide (about 20 amino acids [7]) blocking the channel interacts with the membrane domain near the cytoplasmic end of the pore [8, 9]. It has been suggested that in order to provide access to the pore, T1 must be separate from the membrane domain similar to a hanging gondola [6]. Here, we present the three-dimensional structure of the entire Shaker channel at 2.5 nm resolution, providing further evidence for the hanging gondola model.

Results and Discussion

We expressed Shaker channels in COS cells and purified detergent-solubilized protein on an immunoaffinity column (Figure 1a) using the 1D4 epitope tag [10]. Proper folding, assembly, and stability of the channel were assayed using radiolabeled agitoxin (Figure 1b). Yields (about 1 pmol/plate) were far too low for crystallization trials. However, we obtained sufficient channel protein to observe single channels in an electron microscope. Shaker potassium channels have a combined molecular mass of about 400 kDa (see later), making it difficult to observe them embedded in ice (cryomicroscopy). Therefore, image contrast was enhanced using uranyl acetate negative staining. Single-channel particles are clearly visible in Figure 1c. Most of the particles assumed orientations displaying a mushroom shape. A smaller number of particles assumed other orientations including four-fold symmetrical views (Figure 2a). This distribution of orientations differs substantially from that observed earlier [11]. About 6000 individual images were aligned and classified into 100 classes using IMAGIC [12]. We selected 54 of the strongest classes (illustrated in Figure 2b) for calculation of a three-dimensional (3-D) structure of the channel using angular reconstitution [13]. The structure was further refined using the program

‡To whom correspondence should be addressed (e-mail: niko@brandeis.edu).

Key words: Shaker potassium channel; electron microscopy; single particle analysis

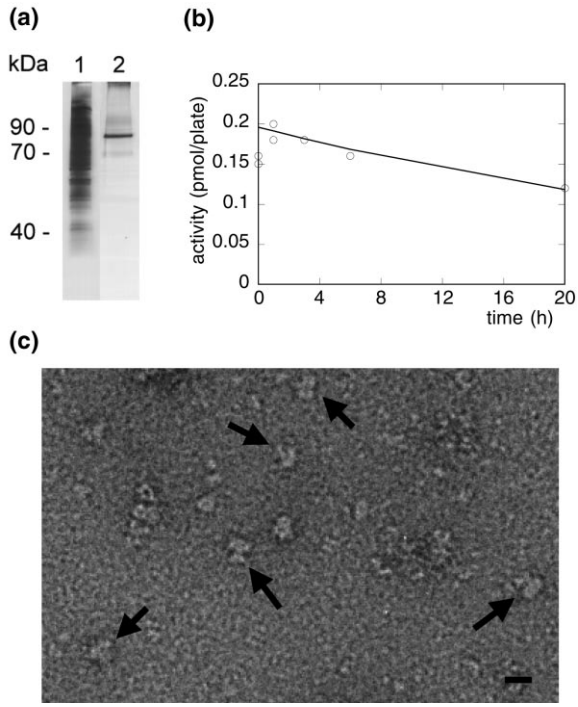

Figure 1. Preparation of Purified Shaker Protein

(a) SDS-PAGE analysis of cell extract (lane 1) and Shaker elution fraction from the immunoaffinity column (lane 2). The main band in lane 2 occurs at about 86 kDa and corresponds to glycosylated channel protein.

(b) Time course of agitoxin binding to purified channel solubilized in CHAPS. The half life of the channel is about 25 hr.

(c) Electron micrograph of purified Shaker protein. Some channels are marked by arrows. Most channels are oriented with their pore axis parallel to the image plane, displaying a mushroom shape where the membrane and T1 domains are visible as separate densities. Scale bar = 10 nm.

FREALIGN [14]. We imposed four-fold symmetry on the structure after verification that the characteristic shape and features were also present in the structure without imposed symmetry (Figure 2d). Figure 3a shows the refined reconstruction of the channel in three different orientations at a resolution of 2.5 nm. The contour level chosen to generate the structure in Figure 3a is based on an average protein density of 810 Da/nm^3 [15] and a volume giving roughly 400 kDa total mass, taking into account the Δ6–46 deletion (see Experimental Procedures) and including glycosylation (approximately 16 kDa per subunit [16]) and bound detergent (about 15 kDa per subunit, estimated by sedimentation [data not shown]). Figure 3b shows 0.35 nm thick slices through the reconstruction perpendicular to the symmetry axis. The density of the slices was mapped above the same threshold used to contour the reconstruction in Figure 3a.

Overall Structure

The structure has a square shape and clearly shows two domains linked by thin connectors about 2 nm long. Based on their volume, the two domains have masses of about 300 kDa and 100 kDa, respectively. The larger domain is about 10 nm across and 6 nm thick. Viewed from the top (Figure 3a, right panel), the large domain shows a central spherical density surrounded by radially arranged crevices, which give the large domain a V-shape. The V-shape leads to an apparent 45° rotation of the density visible in the slices in Figure 3b as the density is mapped from the extracellular end to the cytoplasmic end. The central spherical density lies on the

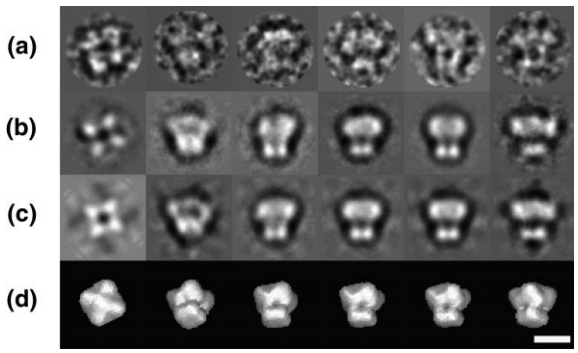

Figure 2. Image Processing of Shaker Images

(a) Some selected images of channels, band-pass filtered and aligned with their respective class average in the same column in the next row.

(b) Some of the 54 class averages used to reconstruct the 3-D structure of the channel. The averages show more detail due to their improved signal-to-noise ratios.

(c) Reprojections of the 3-D structure (before refinement and CTF correction) showing views that match the class averages in (b).

(d) Surface representation of the refined, CTF-corrected 3-D structure shown in orientations corresponding to the reprojections in (c). The structure is shown without imposing four-fold symmetry. Scale bar = 10 nm.

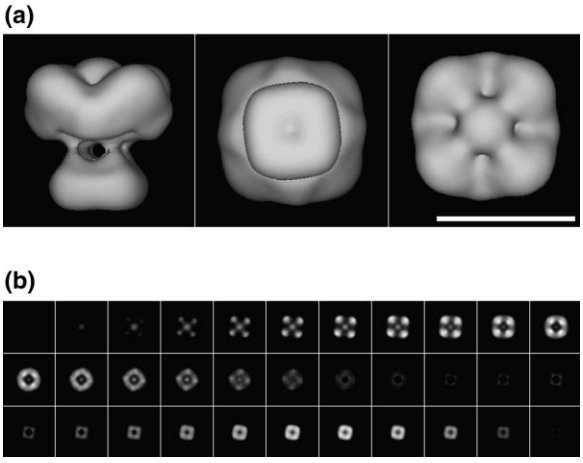

Figure 3. The 3-D Structure of the Shaker Channel

Surface representation of the 3-D structure of Shaker (images produced using WEB [40]).

(a) Three views of the channel in different orientations. From left to right: channel axis in the plane of the image with the membrane domain up and the cytoplasmic domain down (side view), view facing the cytoplasmic domain (bottom view), view facing the membrane domain (top view). A small rotation of the cytoplasmic domain with respect to the membrane domain is visible. Scale bar = 10 nm.

(b) Slices (0.35 nm) through the channel perpendicular to the channel (symmetry) axis. Slices start from the membrane end.

four-fold symmetry axis and, therefore, this part of the density is less reliable, due to the lack of four-fold averaging. The small domain measures approximately 6 nm across and has a thickness of about 3 nm. It is slightly twisted (about 5°) with respect to the large domain (Figure 3a, middle panel), producing a noticeable handedness in the structure. The thin connectors border the sides of putative windows between the two domains. At this contour level, the windows have a long axis of approximately 3 nm perpendicular to the symmetry axis and a short axis of approximately 2 nm parallel to the symmetry axis. A precise measurement of the window dimensions cannot be deduced from our model. First, a resolution of 2.5 nm can affect the measurements. Calculations using models (data not shown) argue that the smallest dimensions still compatible with the observed density profile across the windows are about 2 nm for the long axis and about 1 nm for the short axis (see Experimental Procedures). Second, negative staining sometimes leads to distortions in the protein structure. However, the shape of the observed protein particles is very reproducible, making larger random distortions unlikely. Systematic distortions affecting the total volume of the channel, for example, flattening or partial staining, must also be small since contouring the map to include the estimated total mass of 400 kDa produces a volume and shape that are compatible with the crystal structures of KcsA and the T1 domain (see below).

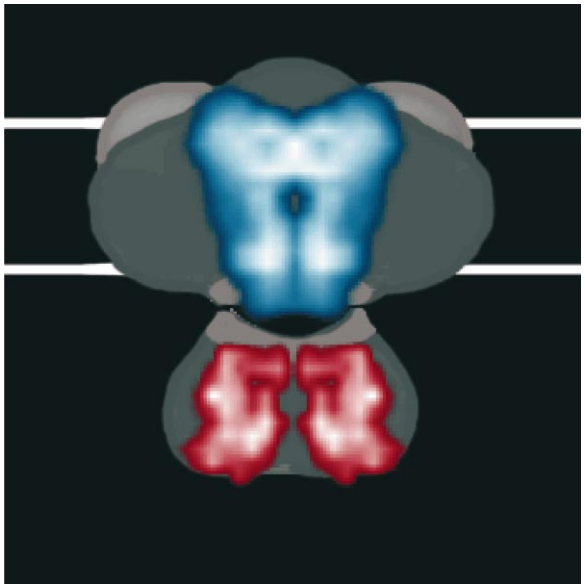

Figure 4. Interpretation of the 3-D Structure of Shaker

The 3-D model shown in Figure 3a has been sliced along the channel axis through the middle of the channel to reveal the outline of the inside of the channel. The atomic structures of the bacterial potassium channel KcsA and the T1 domain are superimposed in blue and red, respectively. The two white lines in the background are 4 nm apart and indicate the approximate position of the lipid bilayer.

Interpretation of Density

This structure is naturally interpreted in terms of the known structure-function relationships of voltage-gated channels. The Shaker polypeptide chain is 656 amino acids long [17], giving it a molecular mass of 74 kDa. The T1 domain includes about 130 residues (approximately residues 98–225) [18–20], and the transmembrane domain consisting of 6 membrane-spanning segments (S1–S6) has been assigned residues 228–478 [17]. The membrane-extrinsic C-terminal end of Shaker includes about 180 amino acids and is located on the cytoplasmic side of the channel. To interpret our 3-D structure, we used the crystal structures of the isolated T1 domain [3] and the KcsA channel [2]. The T1 domain forms a tetramer in the crystal structure, and recently Kobertz and Miller [6] showed that this structure is preserved in the fully assembled channel. KcsA also forms a tetramer with two transmembrane helices per subunit forming the channel pore. The four-fold symmetry of the KcsA and T1 structures demands that both must be positioned on the symmetry axis of the channel. Figure 4 shows slices of the crystal structures rendered at low resolution and superimposed on a cross section of the Shaker structure. The KcsA channel, shown in blue, is too large to fit into the small domain and thus must be placed in the large domain. Therefore, this domain must represent the membrane-intrinsic part of Shaker. With KcsA placed in the large domain, the only other density sufficiently large to accommodate the T1 crystal structure along the four-fold axis is the small domain. In Figure 4, the T1 crystal structure is shown in red and accounts for most of the volume of the small domain. We therefore identify the smaller domain to be the cytoplasmic mass of Shaker containing T1. The orientation of the T1 tetramer has been chosen to agree with the crystal structure of the isolated T1–β-subunit complex [21]. The square shape of the T1 crystal structure coincides with that of the small domain, determining the axial alignment of the T1 structure within the Shaker structure. The orientation of the KcsA structure within the Shaker structure is determined by the intracellular N and C termini. In Figure 4, we placed the KcsA structure in the center of the membrane domain of Shaker. Since KcsA represents only a small part of the membrane domain, its axial alignment cannot be determined from its fit. Therefore, we only show a slice through the rotational average of the KcsA density in Figure 4. However, the dimension of KcsA perpendicular to the membrane is very similar to that of the Shaker membrane domain, in agreement with the expected structural similarity between KcsA and the pore region of Shaker.

The C-terminal end of Shaker includes about 20 kDa per subunit, more than the entire T1 domain (about 15 kDa). However, its conformation is not known. In our 3-D reconstruction, the small domain has a volume corresponding to a mass of about 100 kDa, leaving density corresponding to 40 kDa unaccounted for by the T1 tetramer. It is possible that some of this density is produced by part of the C terminus. Indeed, a close association between the T1 domain and the C terminus is indicated by the fact that the two cysteines at position 96 (T1 domain) and 505 (C terminus) can be cross-linked [22]. Furthermore, we can not interpret the density we ascribe to the membrane domain of Shaker (except for the pore region) due to the lack of an atomic model for

S1–S4. Therefore, part of the large domain could also include density from the C terminus. It is also possible that part of the C terminus does not form a distinct structure but is disordered and is thus not visible in our reconstruction. In this case, the contour level for the surface representation in Figure 3a would be slightly too low but still within the error margins discussed in the Experimental Procedures.

Biological Implications

This paper describes the 3-D structure of a full-length voltage-gated ion channel. By placing the crystal structure of the T1 domain in the low resolution EM map, we are able to determine its approximate position within the channel. The role of the T1 domain has been the subject of much debate. When the isolated T1 tetramer was first crystallized [3], it was suggested that it would form part of the ion conduction pathway of Shaker since it revealed a 0.3 nm hole in the center of the tetramer. However, this interpretation was inconsistent with the binding of the 20 amino acid inactivation peptide close to the pore in the membrane domain of the channel [8]. The 0.3 nm hole in the T1 tetramer is too small to give the inactivation peptide access to the pore. Furthermore, an active role of T1 in ion conduction or pore selectivity appeared unlikely in the light of fully functional channels lacking the T1 domain [23]. It remained unclear how the T1 domain would have to be arranged with respect to the membrane domain and pore to make the pore accessible to ions and the inactivation peptide. One possibility was that T1 would not actually form a tetramer in the fully assembled channel. However, a tetrameric conformation in functional Shaker channels was shown by cross-linking the T1 subunit using designed cross-subunit disulphides [6]. This demanded that T1 be separated from the membrane domain, and a model resembling a hanging gondola was suggested. The interpretation of our low-resolution map confirms this model and provides an approximate distance between T1 and the membrane domain.

The windows separating the membrane and cytoplasmic domains are the most striking part of the structure. A similar structure was recently observed for the acetylcholine receptor (AChR) [24] and the mechanosensitive channel MscL [25] and inferred for full-length KcsA [26], suggesting that the hanging gondola architecture is a common element in ion channels. AChR is a heteropentameric cation-selective channel that shares no homology with Shaker. However, the structure of AChR shows an axial mass on the cytoplasmic side linked to the membrane domain by five connectors. The openings lined by these connectors are about 1.5 nm long and 0.8 nm wide. Unwin and coworkers [24] have suggested that they serve as filters to prevent impermeant molecules from reaching the vicinity of the pore. The windows observed in the Shaker structure are somewhat larger than the openings in the AChR structure, and it is not clear if they have a similar function. However, it was recently proposed that the charge distribution near the windows in Shaker controls access for the inactivation peptide to the pore [21], and thus the windows may indeed act as filters for other molecules.

Recently, it was proposed that T1 participates in channel gating [27, 28]. This is consistent with earlier results showing that phosphorylation of the T1 domain in a Shaker-like channel affects gating [29]. In addition, the T1 domain acts as a docking site for the auxiliary β subunit of voltage-gated ion channels [30, 31], opening up the possibility that gating may also depend on proteins binding to T1 [21]. Our structure implies that participation of T1 in gating must be indirect via the thin connectors separating the T1 domain by 0.2 nm from the membrane domain.

Experimental Procedures

Expression and Purification

We used the inactivation-removed Shaker B channel construct [32] Δ6–46/F425G, which contains a point mutation to affect a 2,000-fold toxin binding enhancement [33]. A 1D4 immunoaffinity tag was added to the C terminus to enable efficient immunoaffinity purification [10]. Channel protein was expressed in COS cells [16] and solubilized at 4°C using 2.5% CHAPS for 1 hr in the presence of 0.5 mg/ml *E.coli* lipid, 1 mM DTT, 0.2 mM leupeptin/pepstatin, and 1 mM PMSF. Insoluble material was pelleted using ultracentrifugation for 45 min at 100,000 $\times$ g. The extract was loaded onto a 1D4 immunoaffinity column in the presence of 5% glycerol and 50 mM NaCl, incubated for 2 hr, washed with wash buffer, and eluted using 1D4 peptide in wash buffer. All buffers contained 80 mM KCl, 2 mM NaEDTA, and 40 mM HEPES-KOH (pH 7.4). Wash buffer also contained 0.7% CHAPS, 1 mM DTT, 50 mM NaCl, 0.2 mM leupeptin/pepstatin, and 1 mM PMSF. The purification has a functional yield of about 30%.

Agitoxin Binding

To quantify correctly folded channels, a channel toxin binding assay was used [33]. We used the charybdotoxin homolog agitoxin (Ag), which has slower off-kinetics. [H^3]NEM-Ag solution was added to the elution fraction to a final concentration of 12.5 nM. Binding was performed at 4°C for 30 min, after which unbounded toxin was separated from the protein–toxin complex using gel filtration on the C-25 SP-Sephadex resin (Sigma). Radioactivity was measured in a liquid scintillation counter.

Electron Microscopy and 3-D Image Processing

Three μl freshly eluted protein was applied to copper grids coated with a thin carbon film after glow-discharging the coated grids. Excess protein was then blotted off, and the grids were washed three times with buffer, followed by three washes in negative stain (1% uranyl acetate). Grids were then examined on a Philips CM12 electron microscope under low-dose conditions to minimize flattening effects. Images were taken at 60,000$\times$ magnification and 1.9 μm underfocus. Forty micrographs were digitized on a SCAI scanner (Zeiss) with a 7 μm pixel size. Groups of 3 $\times$ 3 pixels were then averaged to give 21 μm per pixel on the micrograph, or 0.35 nm on the specimen. Over 6,000 single-channel images were selected manually, and image processing was performed using classification procedures implemented in IMAGIC [12]. We followed a standard protocol (e.g., [34] and references therein). Briefly, the channel images were first band-pass filtered, normalized to have a variance of 10 and an average of 0, and then centered and rotationally aligned against an average of all nonaligned images. A new reference was calculated using the aligned images, and iterations of alignment and averaging were repeated another four times. Aligned images were subjected to multivariate statistical analysis (MSA) [35, 36], where each image is represented as a point in a multidimensional space. MSA determines the new coordinate system where each aligned image can be expressed as a linear combination of independent eigenimages, from which only low-order components are significant and represent systematic variations through the image data set. The higher order components usually are disregarded to reduce noise. MSA-treated images were classified using their eigenimage components, and class averages showing different views of the

channel were obtained after summing all images in each class. The averages of the best classes (largest number of images, lowest variance) were then used as new references for multi reference alignment (MRA) [37]. For each particle image in a data set, MRA finds the best matching reference from a set of references. MRA leads to different alignments for particles with different orientations that can then be separated efficiently using another cycle of MSA and classification. We performed four cycles of MRA, MSA, and classification. Using angular reconstitution [13], the relative orientations of the final class averages were determined and a 3-D reconstruction with imposed four-fold symmetry was calculated using the exact filter back projection algorithm [38]. We also calculated a 3-D reconstruction without imposing four-fold symmetry, confirming that the reconstruction still displayed quasi four-fold symmetry. Reprojections of the first 3-D reconstruction were then used in further MRA. Stable classes were obtained after six iterations of alignment and reconstruction.

The channel orientations were then further refined, and the 3-D reconstruction was corrected for the contrast transfer function (CTF) of the electron microscope using the program FREALIGN [14]. FREALIGN uses an automatic weighting scheme that reduces the weight of images contributing to the final 3-D structure according to their phase residual with respect to the reference structure. Above a certain phase residual threshold, particles are discarded completely. In our refinement, this threshold was set to discard about 20% of the particles. This ensures that after a few cycles of refinement, the structure converges to a point of self-consistency, where it represents the main body of the data set. No further improvement in the reconstruction was observed after 25 iterations using FREALIGN, yielding the final reconstruction. The resolution of the reconstruction was estimated by the Fourier shell correlation (FSC) coefficient [38], with the resolution limit taken at the point where the FSC fell below 0.5 [39]. The measured resolution (2.5 nm) coincides with the approximate position of the first CTF zero, and the reconstruction was filtered to that resolution using a Gaussian function.

Window Size Measurement

The actual size of the windows is uncertain for several reasons. It is possible that there is protein projecting sparsely from the connectors into the windows, which would produce density below the contour level used to render the surface of the structure. This additional protein would make the windows smaller than they appear in Figure 3a. Furthermore, the measured size of the windows depends on the contour level chosen for the reconstruction. This may be an additional source of error since, apart from a small uncertainty in the total mass of protein and detergent, there may also be an inaccuracy in the magnification of the images, typically less than 5%. A 5% error in the magnification would result in a 16% error in the volume measurement. However, if we assume that the space between the connectors is strictly an aqueous cavity, as inferred from electrophysiological measurements [6, 21], we may determine the smallest window size from the density profiles across the windows. Thus, the density profile (data not shown) crossing two connectors on either side of a window (long axis) is consistent with a separation of the connectors of at least 2 nm. The density profile across a window along the symmetry axis (short axis) is consistent with a separation of the membrane and cytoplasmic domain of at least 1 nm.

Acknowledgments

The Shaker channel construct is the generous donation of C. Miller. We are also grateful to D. Oprian for providing 1D4 antibodies. The authors would like to thank C. Miller for advice regarding expression and purification of Shaker and for a critical review of the manuscript. The help of Carole Williams and Tania Shahid in maintaining cell cultures is gratefully acknowledged. O. S. receives support from the Jane Coffin Childs Memorial Fund for Medical Research.

Received: October 19, 2000
Revised: December 18, 2000
Accepted: January 10, 2001

References

1. Sigworth, F.J. (1994). Voltage gating of ion channels. Q. Rev. Biophys. *27*, 1–40.
2. Doyle, D.A., et al., and MacKinnon, R. (1998). The structure of the potassium channel: molecular basis of K^+ conduction and selectivity. Science *280*, 69–76.
3. Kreusch, A., Pfaffinger, P.J., Stevens, C.F., and Choe, S. (1998). Crystal structure of the tetramerization domain of the Shaker potassium channel. Nature *392*, 945–948.
4. Roux, B., and MacKinnon, R. (1999). The cavity and pore helices of the KcsA K+ channel: electrostatic stabilization of monovalent cations. Science *285*, 100–102.
5. Tu, L.W., Santarelli, V., and Deutsch, C. (1995). Truncated K+ channel DNA-sequences specifically suppress lymphocyte K+ channel gene-expression. Biophys. J. *68*, 147–156.
6. Kobertz, W.R., Williams, C., and Miller, C. (2000). Hanging gondola structure of the T1 domain in a Shaker K^+ channel. Biochemistry *39*, 10347–10352.
7. Hoshi, T., Zagotta, W.N., and Aldrich, R.W. (1990). Biophysical and molecular mechanisms of Shaker potassium channel inactivation. Science *250*, 533–538.
8. Isacoff, E.Y., Jan, Y.N., and Jan, L.Y. (1991). Putative receptor for the cytoplasmic inactivation gate in the Shaker K^+ channel. Nature *353*, 86–90.
9. del Camino, D., Holmgren, M., Liu, Y., and Yellen, G. (2000). Blocker protection in the pore of a voltage-gated K^+ channel and its structural implications. Nature *403*, 321–325.
10. Oprian, D.D., Molday, R.S., Kaufman, R.J., and Khorana, H.G. (1987). Expression of a synthetic bovine rhodopsin gene in monkey kidney-cells. Proc. Natl. Acad. Sci. USA *84*, 8874–8878.
11. Li, M., Unwin, N., Stauffer, K.A., Jan, Y.N., and Jan, L.Y. (1994). Images of purified Shaker potassium channels. Curr. Biol. *4*, 110–115.
12. van Heel, M., Harauz, G., Orlova, E.V., Schmidt, R., and Schatz, M. (1996). A new generation of IMAGIC image processing system. J. Struct. Biol. *116*, 17–24.
13. van Heel, M. (1987). Angular reconstitution: a posteriori assignment of projection directions for 3D reconstruction. Ultramicroscopy *21*, 111–124.
14. Grigorieff, N. (1998). Three-dimensional structure of bovine NADH:ubiquinone oxidoreductase (complex I) at 22 Å in ice. J. Mol. Biol. *277*, 1033–1046.
15. Matthews, B.W. (1968). Solvent content of protein crystals. J. Mol. Biol *33*, 491–497.
16. Sun, T., Naini, A.A., and Miller, C. (1994). High-level expression and functional reconstitution of Shaker K^+ channels. Biochemistry *33*, 9992–9999.
17. Schwarz, T.L., Tempel, B.L., Papazian, D.M., Jan, Y.N., and Jan, L.-Y. (1988). Multiple potassium-channel components are produced by alternative splicing at the Shaker locus in Drosophila. Nature *331*, 137–142.
18. Li, M., Jan, Y.N., and Jan, L.Y. (1992). Specification of subunit assembly by the hydrophilic amino-terminal domain of the shaker potassium channel. Science *257*, 1225–1230.
19. Shen, N.V., and Pfaffinger, P.J. (1995). Molecular recognition and assembly sequences involved in the subfamily-specific assembly of voltage-gated K^+ channel subunit proteins. Neuron *14*, 625–633.
20. Bixby, K.A., et al., and Choe, S. (1999). Zn^{2+}-binding and molecular determinants of tetramerization in voltage-gated K^+ channels. Nat. Struct. Biol *6*, 38–43.
21. Gulbis, J.M., Zhou, M., Mann, S., and MacKinnon, R. (2000). Structure of the cytoplasmic β subunit-T1 assembly of voltage-dependent K^+ channels. Science *289*, 123–127.
22. Schulteis, C.T., Nagaya, N., and Papazian, D.M. (1996). Intersubunit interaction between amino- and carboxyl-terminal cysteine residues in tetrameric Shaker K^+ channels. Biochemistry *35*, 12133–12140.
23. Kobertz, W.R., and Miller, C. (1999). K+ channels lacking the "tetramerization" domain: implications for pore structure. Nat. Struct. Biol *6*, 1122–1125.
24. Miyazawa, A., Fujiyoshi, Y., Stowell, M., and Unwin, N. (1999). Nicotinic acetylcholine receptor at 4.6 Å resolution: transverse tunnels in the channel wall. J. Mol. Biol *288*, 765–786.

25. Chang, G., Spencer, R.H., Lee, A.T., Barclay, M.T., and Rees, D.C. (1998). Structure of the MscL homolog from Mycobacterium tuberculosis: a gated mechanosensitive ion channel. Science *282*, 2220–2226.
26. Cortes, D.M., Cuello, L.G., and Perozo, E. (2000). Molecular architecture of full-length KcsA: role of cytoplasmic domains in ion permeation and activation gating. J. Gen. Physiol., in press.
27. Cushman, S.J., Nanao, M.H., Jahng, A.W., DeRubeis, D., Choe, S., and Pfaffinger, P.J. (2000). Voltage dependent activation of potassium channels is coupled to T1 domain structure. Nat. Struct. Biol. *7*, 403–407.
28. Minor, D.L., et al., and Berger, J.M. (2000). The polar T1 interface is linked to conformational changes that open the voltage-gated potassium channel. Cell *102*, 657–670.
29. Huang, X.Y., Morielli, A.D., and Peralta, E.G. (1994). Molecular basis of cardiac potassium channel stimulation by protein kinase A. Proc. Natl. Acad. Sci. USA *91*, 624–628.
30. Sewing, S., Roeper, J., and Pongs, O. (1996). Kv beta 1 subunit binding specific for shaker-related potassium channel alpha subunits. Neuron *16*, 455–463.
31. Yu, W., Xu, J., and Li, M. (1996). NAB domain is essential for the subunit assembly of both alpha-alpha and alpha-beta complexes of shaker-like potassium channels. Neuron *16*, 441–453.
32. Zagotta, W.N., Hoshi, T., and Aldrich, R.W. (1990). Restoration of inactivation in mutants of Shaker potassium channels by a peptide derived from ShB. Science *250*, 568–571.
33. Goldstein, S.A.N., and Miller, C. (1992). A point mutation in a Shaker K^+ channel changes its chaybdotoxin binding site from low to high affinity. Biophys. J. *62*, 5–7.
34. Orlova, E.V., et al., and van Heel, M. (1997). Structure of keyhole limpet hemocyanine Type 1 (KLH1) at 15 Å resolution by electron cryomicroscopy and angular reconstitution. J. Mol. Biol. *271*, 417–437.
35. van Heel, M., and Frank, J. (1981). Use of multivariate statistics in analyzing the images of biological macromolecules. Ultramicroscopy *6*, 187–194.
36. van Heel, M. (1984). Multivariate statistical classification of noisy images (randomly oriented biological macromolecules). Ultramicroscopy *7*, 165–183.
37. van Heel, M., and Stöffer-Meilicke, M. (1985). Characteristic views of the *E. coli* and *B. stearothermophilus* 30S ribosomal subunits in the electron microscope. EMBO J. *4*, 2389–2395.
38. Harauz, G., and van Heel, M. (1986). Exact filters for general geometry three-dimensional reconstruction. Optik *73*, 146–156.
39. Böttcher, B., Wynne, S.A., and Crowther, R.A. (1997). Determination of the fold of the core protein of hepatitis B virus by electron microscopy. Nature *386*, 88–91.
40. Frank, J., et al., and Leith, A. (1996). SPIDER and WEB: processing and visualization of images in 3-D electron microscopy and related fields. J. Struct. Biol. *116*, 190–199.